A Mechanistic Study of the Li-air Battery with Co_3O_4 Cathode and DMSO Electrolyte

Zhen Jiang[a] and Andrew M. Rappe[a*]

[a]*Department of Chemistry, University of Pennsylvania, Philadelphia, PA, 19104–6323 USA*

E-mail: rappe@sas.upenn.edu

Abstract

The lithium-air battery, a powerful competitor to replace the traditional lithium-ion battery, has attracted increasing attention due to its extremely high theoretical energy density. However, development is limited by the cathode and electrolyte properties, which should include high stability, conductivity, and electrocatalytic properties in oxygen-rich environments. Here, we employ a systematic first-principles study of Li-O_2 discharge and charge reactions on the Co_3O_4-based cathode with the assistance of DMSO electrolyte. The structure, stability, and electronic properties of different surface reconstructions of the Co_3O_4 (100) facet are investigated. In addition, the mechanisms and thermodynamic overpotetials of multi-step reactions between Li^+/e^- and O_2 are provided, where lithium suboxide products (Li_2O_2 or Li_3O_2) are formed on the different Co_3O_4 (100) terminations. The solvation shell of Li^+ components in explicit DMSO solvent are investigated through *ab initio* molecular dynamics (AIMD) simulations. In general, we find that the Co_3O_4 (100)-O (Oxidized) surface is the most stable one at standard conditions, and the stable Li^+ solvation structure is found in a tetrahedral $Li(DMSO)_4^+$ shell in the DMSO-based electrolyte. Moreover, in the system of Co_3O_4 (100)-O cathode and DMSO electrolyte, the solution model pathway is energetically favorable for Li-O_2 discharge reaction. It provides a low constant

overpotential of 0.17 V during a long-term discharging process, thus causing the final toroid Li_2O_2 formation on the cathode. During the charging process, the overpotential of 0.36 V is required to rapidly decompose the Li_2O_2.

Introduction

Recently, the great commercial value and environmental friendly properties of battery electric vehicles (BEVs) have attracted the attention of many companies. However, the development is limited by the energy storage technology.[1–4] The current rechargeable batteries are based on Li-ion batteries (LIBs), which offer usable energy of up to 120 W·h/kg. In order to give a car a range of 200–300 miles, an ideal energy capacity of ≈75 kW·h is required on a single charge.[5–7] Based on that, a very heavy battery (625 kg) is required on the vehicle, which will reduce its energy efficiency. Therefore, it is compelling to search for other battery designs to enhance BEVs. Among many candidates, the Li-air battery is a promising energy storage paradigm which can theoretically provide a specific energy of nearly 12.0 kW·h/kg (100 times the capacity of LIBs).[8–11] However, the current Li-air batteries can only provide a practical energy of 1.7 kW·h/kg, which is limited by many factors including cathode materials. Therefore, more systematic studies of Li-air batteries are needed. The overall discharge and charge reactions of the Li-air battery are[12–14]

$$2Li^+ + 2e^- + O_2(g) \underset{\text{charge}}{\overset{\text{discharge}}{\rightleftharpoons}} Li_2O_2, E^0 = 2.96 \text{ V}. \quad (1)$$

$$4Li^+ + 4e^- + O_2(g) \underset{\text{charge}}{\overset{\text{discharge}}{\rightleftharpoons}} 2Li_2O, E^0 = 2.91 \text{ V}. \quad (2)$$

Although the Li_2O discharge product in reaction (2) delivers higher energy density, breaking the O–O bond makes this reaction slow and possibly irreversible. Therefore, most of the current cathodes can only provide Li_2O_2 as a product following reaction (1).[15,16] To date, Co_3O_4 is one of the most popular cathodes among metal oxides for Li-air batteries, since it

is active, conductive, and stable under the O_2 rich environment.[17–19] Moreover, according to the experimental reports, it can provide a low discharge overpotential during operation.[20] However, the mechanism of charge and discharge reactions on the Co_3O_4 cathode is still unknown. Therefore, it is important to provide a systematic first-principles study of the roles of the Co_3O_4 cathode towards Li-O_2 reactions.

The structure and stability of Co_3O_4 have been studied experimentally and theoretically.[18,21,22] Co_3O_4 is an antiferromagnetic spinel oxide, including tetrahedrally-coordinated Co^{2+} (magnetic moment = 3.0 μ_B in experiment, 2.69 μ_B in density functional theory, DFT) and octahedrally-coordinated Co^{3+} (0 μ_B) ions.[22] The (100), (110), and (111) surfaces are the most prevalent facets exposed on Co_3O_4 based on previous observations.[23,24] Among these, the (100) facet has been confirmed to be most stable by DFT calculations and is considered to be the main/only facet in many sustainable catalytic processes.[22,25] However, even for the (100) surface, there are three different symmetric pristine terminations, which are usually named as (100)-O (oxidized), (100)-S (stoichiometric), and (100)-R (reduced) surfaces depending on the surface Co:O ratio (see Fig. 1(c)-(e)). It was reported that the (100)-O surface is the most stable one in the standard conditions (T^0=298.15 K, $P^0_{O_2}$ = 0.21 atm).[22,25] However, the surface reconstruction behavior of the (100)-O facet, such as O or Co vacancy formation, has not been studied extensively. In addition, the electronic properties of these three surfaces have not be examined. Therefore, it is important to investigate the surface stability, properties, and reconstructions of a Co_3O_4 (100) slab systematically before simulating the Li-O_2 reactions on it.

The mechanism and product growth pathways for the Li-O_2 discharge and charge reactions on Co_3O_4 are still unknown. The superiority of Co_3O_4 as a cathode relative to other transition-metal oxides is due to low discharge and charge overpotentials ($\eta_{discharge} \approx$ 0.1-0.3 V, $\eta_{charge} \approx$ 1 V) reported experimentally.[16,20] However, the current Co_3O_4-based battery still must be improved in both discharge and charge processes. Therefore, a systematic *ab initio* study is necessary to unveil the potential- and rate-determining steps for the multiple

electron transfer steps in the overall Li-O_2 reactions. It is also notable that most theoretical calculations simulated the thin-film growth of Li_2O_2 discharge product on the cathodes, which should reduce catalytic activity from that of Co_3O_4 to that of Li_2O_2 (s). However, this surface deactivation phenomenon is often ignored.[26–29] Indeed, on some recently-proposed Li-air battery electrodes, toroid shaped Li_2O_2 nanoparticles were found after discharge (not blocking the electrode active sites).[10,30,31] The morphology change from thin film to toroid shape is attributed to the use of different electrolytes, thus indicating two different Li_2O_2 growth pathways: the surface and solution models.[32,33]

Surface model:

$$2Li^+ + 2e^- + O_2(g) \xrightarrow{\text{discharge}} Li_2O_2(s)$$

Solution model:

$$Li^+ + e^- + O_2(g) \xrightarrow{\text{discharge}} LiO_2(s) \quad \text{(a)}$$

$$LiO_2(s) \xrightarrow{\text{desorption}} LiO_2(sol) \quad \text{(b)}$$

$$2LiO_2(sol) \xrightarrow{\text{condensation}} Li_2O_2(s) + O_2(g) \quad \text{(c)}$$

In the surface model, all Li-O_2 reactions are completed on the cathode surface, resulting in thin-film discharge products. Regarding the solution model, the soluble LiO_2 intermediates form via reaction (a) and then desorb from the cathode surface into the electrolyte (reaction (b)), followed by two LiO_2 disproportionating into insoluble Li_2O_2 on the cathode surface (in a toroid-shaped particle) (reaction (c)). The discrimination of the two growth models is mainly influenced by the LiO_2 desorption ability at the interface, which is closely determined by the donor number (*i.e.* Lewis basicity) of the electrolyte.[32,33] The donor number is a representative parameter to indicate the ability of a solvent to solvate cations and small molecules by donating an electron pair, where a higher donor number relates to higher solubility. Recently, the solution model has become more important than the surface

model in Li-air batteries because it can continuously provide a clean catalytic surface for the discharge reactions, yielding a low and constant discharge overpotential for a long time. Dimethyl sulfoxide (DMSO) is nearly always employed as the supporting electrolyte in recent designs of Li-air batteries to facilitate the solution model discharge pathway.[10,33,34] Therefore, we investigate the roles of Co_3O_4 facets and DMSO electrolyte toward Li-O_2 reactions from a first-principles DFT perspective. In this paper, we present a systematic first-principles study of the stability and reconstruction of Co_3O_4 (100) facets, Li-O_2 reaction mechanisms and overpotentials, solvation structures of Li salts ($LiClO_4$) in DMSO, Li desolvation process at the Co_3O_4/DMSO interface, and pathways for discharge product growth on the Co_3O_4 cathodes.

Results and Discussion

Bulk Co_3O_4 The optimized lattice parameter of cubic Co_3O_4 is 8.18 Å, in agreement with previous DFT and experimental studies (Fig. S1(a)).[22,25] The ground state of Co_3O_4 is antiferromagnetic, where the magnetic moment of the octahedrally-coordinated Co^{3+} is 0 μ_B, while the magnetic moment of the tetrahedrally-coordinated Co^{2+} is 2.65 μ_B. The calculated electronic structure of bulk Co_3O_4 shows it to be a semiconductor with a band gap of 1.75 eV (Fig. 1(a)), which is comparable with the previous experimental and theoretical values ≈1.6–1.7 eV.[22,25]

Table 1: Surface energy and surface band gap of Co_3O_4(100)-O, -S, -R slabs

Surfaces	Φ_G(J/m^2)	Band gap (eV)
(100)-O	1.26	0.20
(100)-S	1.48	0.30
(100)-R	1.61	0

Co_3O_4 (100) surface We start the simulation from three high-symmetry terminations, the Co_3O_4 (100)-O, (100)-S, and (100)-R surfaces (Fig. S1(b)). The optimized surface con-

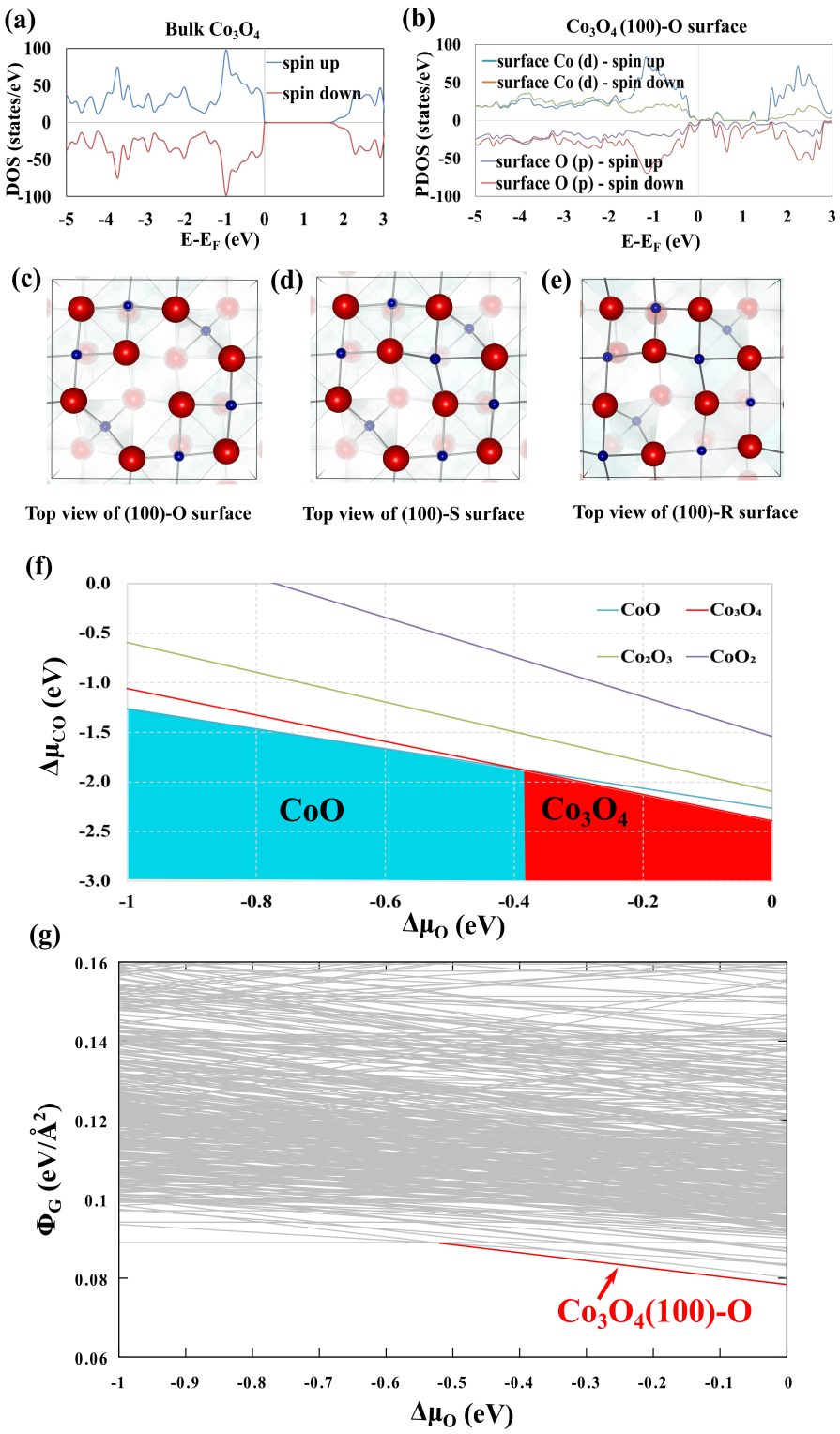

Figure 1: (a), Density of states (DOS) of bulk Co_3O_4, (b) Projected density of states (PDOS) of the Co_3O_4(100)-O surface. (c)-(e): the top view of the Co_3O_4(100)-O, -S, -R surfaces. (f) Phase diagram of bulk CoO, Co_3O_4, Co_2O_3, and CoO_2. (g) Surface energy diagram of 500 reconstructed terminations of Co_3O_4(100) obtained from *ai*-GCMC.

figurations are shown in Fig. 1 (c)-(e), while the surface energies can be found in Table 1. We found that Co_3O_4 (100)-O surface is the most stable one with the lowest surface energy at $T^0 = 298.15$ K and $P^0_{O_2} = 0.21$ atm, and all conditions under which bulk Co_3O_4 is stable. As shown in Fig. 1(c), the top layer is filled by octahedral Co^{3+} with one dangling bond, resulting in a pronounced change of magnetic moment from 0 to 2.0 μ_B. As for the (100)-S or (100)-R surfaces, one or two tetrahedral Co atoms are initially added (per unit cell) onto the top layer of the (100)-O surface (see Fig. S1(b)). After optimization, the tetrahedral Co atoms are shifted into the square surface site formed by four adjacent O atoms, while the magnetic moment remains large, 2.6 μ_B. In addition, according to the electronic structure of the three terminations, the (100)-O and (100)-S facet remains a semiconductor, but the surface bands have a small bandgap of 0.2 (Fig. 1(b)) and 0.3 eV, respectively (Table 1). As for (100)-R surfaces, the surface is metallic.

Next, we consider more reconstruction possibilities of the Co_3O_4 (100) surface by using the *ai*-GCMC method.[35] Co and O atoms will be moved, inserted, or deleted from the surface during the simulation. We start from the Co_3O_4 (100)-O surface, which is determined as the most stable high-symmetry surface (see previous paragraph). The surface energy (grand potential Φ_G $T = 0$, equation in Supporting Information) of all configurations obtained from the *ai*-GCMC simulation are plotted in Fig. 1(g) as a function of $\Delta\mu_O$. We find that the Co_3O_4 (100)-O surface is still the most stable one in the range of $\Delta\mu_O$ = -0.5 eV–0 eV, covering the $\Delta\mu_O$ range for bulk Co_3O_4 stability ($\Delta\mu_O$ = -0.38 eV–0 eV, Fig. 1(f)). All the reconstructed surfaces, including adding more Co/O atoms or making Co/O vacancies are found to be unfavorable. Therefore, we can conclude that Co_3O_4 (100)-O surface is the predominant facet for Co_3O_4 particles. In addition, when the $\Delta\mu_O$ was decreased beyond the bulk stability region, the Co_3O_4 (100)-S and -R surfaces are stable (despite bulk metastability), which is in agreement with previous DFT reports.[25,36,37] Therefore, we systematically studied the catalytic activity of the Co_3O_4 (100)-O facet for Li-O_2 reactions (see below sections), while the catalytic performance of Co_3O_4 (100)-S,-R surfaces can be found

in Supporting Information.

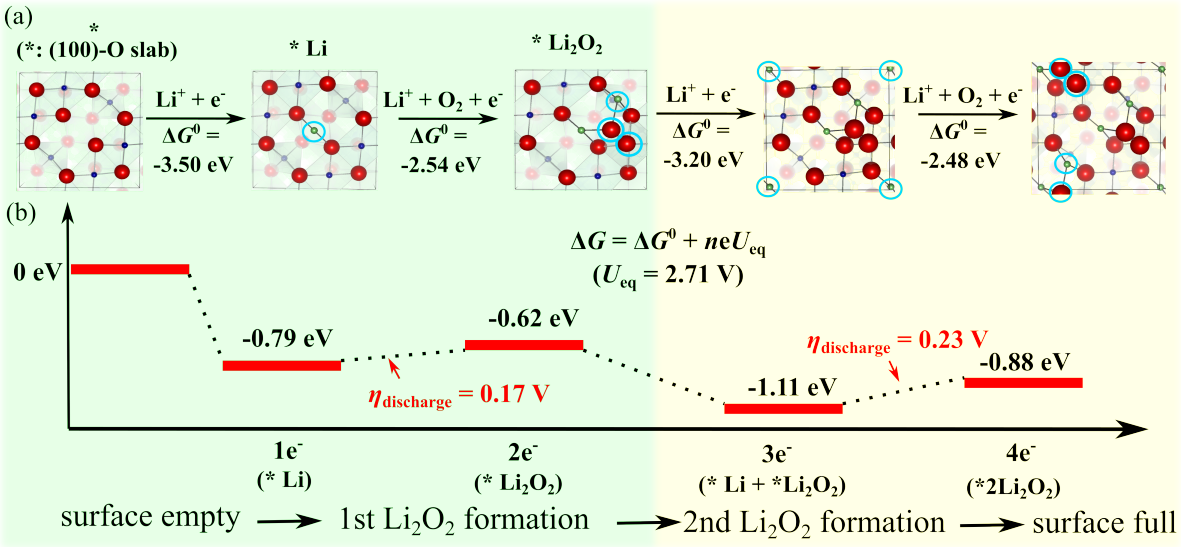

Figure 2: (a) The most thermodynamically favourable formation mechanisms of Li_2O_2 monomers on the Co_3O_4 (100)-O surface. * denotes an adsorption site, and pre-pended * denotes an adsorbed species, *e.g.* *Li. During each step, the newly adsorbed Li and O_2 are circled in sky blue. (b) The free-energy diagram of Li^+/e^- and O_2 reactions on the Co_3O_4 (100)-O surface at the ideal equilibrium potential U_{eq} = 2.71 V, where the $\eta_{discharge}$ for the formation of first and second *Li_2O_2 (per surface cell) are shown.

Thermodynamic overpotential study of Li-O_2 reactions on the Co_3O_4 (100)-O surface Fig. 2 shows the most favourable mechanistic and thermodynamic performance for the discharge reaction between Li^+/e^- and O_2 on the Co_3O_4 (100)-O surface. The effect of DMSO solvent can be ignored when we calculate the theoretical overpotentials in Fig. 2, based on the model of computational lithium electrode provided by Nøskov's group.[38] Because the solvation reactions are not redox reactions, the electrolyte contribution affects the barriers of interfacial adsorption/desorption reactions through the pre-factor of the rate expression (kinetic calculations), but not the potential dependent thermodynamics in this study.[38] In addition, the DFT-defined reference free energy of Li^+/e^- (transfer components during charging and discharging) is computed from the bulk Li-metal (anode material) in this method,[38–40] while lithium ions in solution are assumed in equilibrium with the lithium metal anode and with Li^+ near the cathode surface.[38] Therefore, the solvation effect on the

calculations of Li^+/e^- transfer reaction is quite small, and can be ignored in the estimation of overall discharging/charging reactions between Li-anode and cathode surface.[38] Using this model, we derived DFT-level overpotentials as shown in Fig. 2. The same method has been well tested by many theorists on other electrode materials, obtaining very good estimates of DFT-level overpotentials compared with experiments.[10,29,39–41] Therefore, our DFT-derived overpotentials (in Fig. 2) can be directly compared with other computationally estimated overpotentials on various materials in this Li-air battery field.

As shown in Fig. 2, the initial Li^+/e^- adsorption is extremely exothermic, with ΔG^0 = -3.50 eV. The Li cation will be adsorbed on a bridge site equidistant between two surface O anions, where there is no tetrahedral Co ion directly below in the top subsurface layer. Then, the second pair of Li^+/e^- will be transferred to the neighboring O-O bridge site (right above the subsurface tetrahedral Co), while the O_2 is bonded to the adjacent Co atom on the surface eliminating the dangling bond of a surface Co (by forming a new Co-O bond). By that, the first $*Li_2O_2$ is formed. Another less favourable mechanism to form one $*Li_2O_2$ can be found in Fig. S2, which is also based on the *Li intermediate. We also considered the pathways based on the $*LiO_2$ intermediate (assumed by many experiments). However, for this cathode we found that the Gibbs free energy (ΔG^0 = -3.50 eV) of *Li formation is more favorable than that (ΔG^0 = -2.99 eV) of $*LiO_2$ formation after the first electron transfer step. In addition, we also find the free energy of the O_2 adsorption reaction (*Li(s) + O_2 (g) $\rightarrow$ $*LiO_2$) is ΔG^0 = 0.51 eV, while the Gibbs free energy of *Li(s) + Li^+ + e^- $\rightarrow$ *2Li (s) is ΔG^0 = -0.20 eV (at U_{eq} = 2.71 V). Therefore, we know that the second *Li formation will proceed before the adsorption of O_2, avoiding the existence of $*LiO_2$ intermediate on the Co_3O_4 (100)-O surface. The same pathway (without $*LiO_2$ intermediate formation) has also been found for Li-O_2 reactions on the CeO_2 surface in another study.[41] After the first monomer formation, the remaining half of the active sites (Co and O-O bridge sites) on the Co_3O_4 (100)-O surface can provide an energetically favourable pathway to form a second $*Li_2O_2$ (per surface cell) with the same mechanism in the first $*Li_2O_2$. The formation energy

of the second *Li_2O_2 is a bit less exothermic due to the steric hindrance from the first *Li_2O_2. After the second *Li_2O_2 formation, the surface (of our simulation model, 8.18 × 8.18 Å^2) is fully covered by Li_2O_2(s), and there are no active O-O bridge sites left for additional Li^+ adsorption. The free-energy diagram for Li-O_2 reactions on the Co_3O_4(100)-O surface is plotted at the ideal equilibrium potential U_{eq} =2.71 V (Fig. 2(b)). As shown, the discharge potential-determining step (PDS) is the second step (*Li + Li^+ + e^- + O_2 → *Li_2O_2) with overpotentials (making all steps downhill) of 0.17 V and 0.23 V for the formation of both first and second *Li_2O_2, respectively.

The effect of DMSO solvent towards the Li-O_2 reactions. Here, we consider the solvation effects of DMSO towards the configurations in Fig. 2(a). The first step is to obtain the structural properties of Li^+ and O_2 in DMSO solvent. ClO_4^- is also added into the simulations as the counter ion, because $LiClO_4$ is believed as the most stable Li salt.[34] Fig. 3(a) shows a well-equilibrated first solvation shell of Li^+ in DMSO solvent from 25 ps *ab initio* molecular dynamics (AIMD) simulations (10 ps equilibration, and 15 ps production run) and post-statistical analysis. The Li^+ component is observed in a stable tetrahedral structure with four DMSO molecules as coordinates, where O atoms in DMSO act as the coordinating sites. The averaged distance of four Li-O bonds in the $Li(DMSO)_4^+$ solvation shell is 2.04 Å from 15 ps production run. This well-defined tetrahedral $Li(DMSO)_4^+$ solvation structure also corresponds to the running coordination number (red line in Fig. 3(b)) keeping at four in the $d_{Li-O_{DMSO}}$ range from 2.0 to 4.0 Å. The distance evolution of Li^+-O (from O_2) bonds and Li^+-Cl (from ClO_4) bond are also plotted in Fig. 3(c). As shown, the d_{Li-O} mainly fluctuates above 4.0 Å (4.97 Å in average) and d_{Li-Cl} generally fluctuates above 6.0 Å (7.11 Å in average). All the above AIMD analysis confirms that the $Li(DMSO)_4^+$ configuration is the stable solvation shell for Li^+ component in DMSO electrolyte, which is taken into the adsorption (desolvation) reaction simulations at the Co_3O_4 (100)-O/DMSO (electrode/electrolyte) interface in the following paragraph.

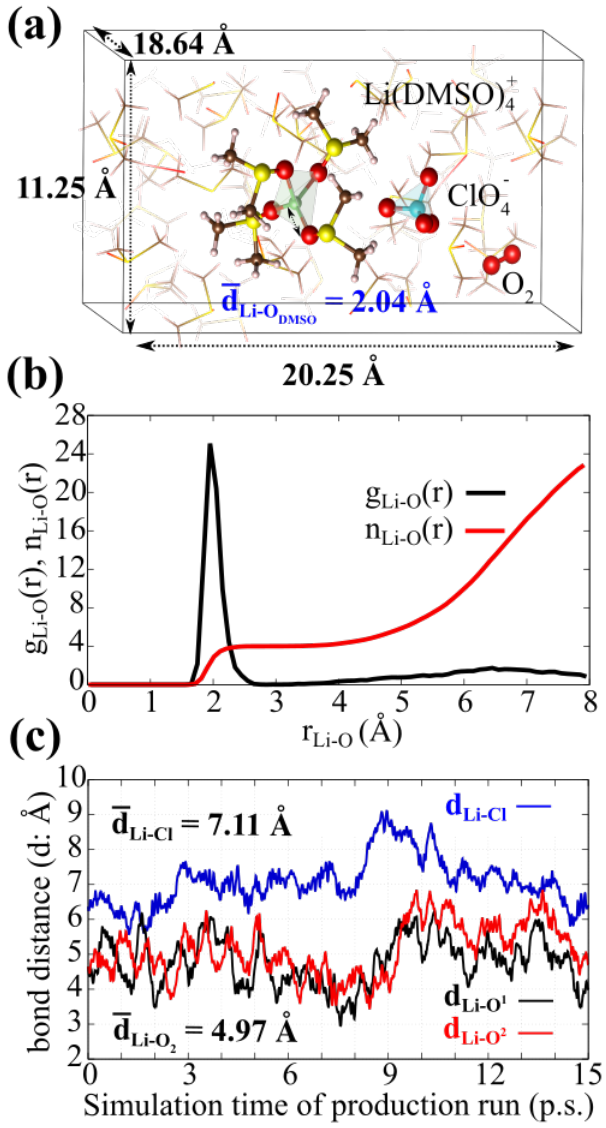

Figure 3: (a), Simulation box created for one pair of Li^+ and ClO_4^- ions and O_2 molecule in the explicit DMSO solvents. The equilibrated tetrahedral $Li(DMSO)_4^+$ structure is shown as the obtained stable first solvation shell, together with the averaged bond distance between Li^+ and O atoms (O from the four DMSO coordinates). (b) Partial Li-O radial distribution function (RDF) ($g_{Li-O}(r)$) and running coordination number ($n_{Li-O}(r)$) for Li^+ in DMSO solvents. (c) Bond distance evolution of Li-Cl (from ClO_4^-), Li-O^1 and Li-O^2 (from O_2) during the 15 ps AIMD production run in the explicit DMSO solvent.

Fig. 4 shows a systematic comparison of the adsorption configurations for an explicit $Li(DMSO)_4^+$ solvation shell on the Co_3O_4 (100)-O surface. Compared with the outer-sphere structure (Fig 4(a)), *$Li(DMSO)_3$ is thermodynamically unfavourable (ΔG^0 = 1.41 eV) to be adsorbed on the top site of surface O atom (Fig 4(b)). All the other three inner-sphere adsorptions are found thermodynamically favourable, where Li atoms (coordinated with 0, 1, or 2 DMSO ligands) are located on the O-O bridge site of the Co_3O_4 (100)-O surface. Among them, the *Li(DMSO) adsorbate in Fig 4(d) is the most favourable configuration ((ΔG^0 = -1.04 eV)). Therefore, we confirmed that the Li^+/e^- will be transferred on the surface O-O bridge site (without subsurface tetrahedral Co) of Co_3O_4 (100)-O surface as shown in Fig. 2. Here, it is notable that although the effect of one DMSO ligand (binding to *Li) are ignored when we calculate theoretical overpotentials in Fig. 2, thus derived overpotentials can still provide a reasonable prediction. The detailed explanation can be found in the above section of thermodynamic overpotential study. After that, the DMSO ligand (in Fig 4(d)) can be released by the further O_2 adsorption on top of this *Li to form the final Li_2O_2 products.

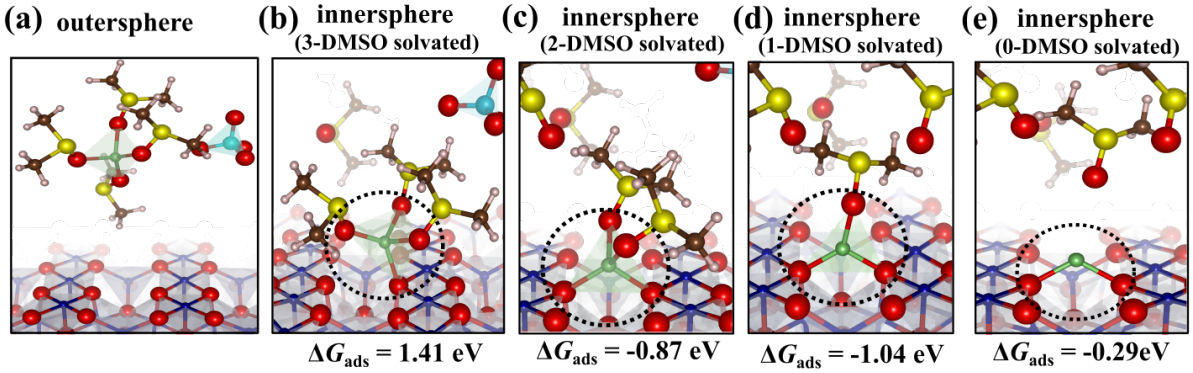

Figure 4: (a), The outer-sphere structure of $Li(DMSO)_4^+$ solvation shell and ClO_4^- on the Co_3O_4 (100)-O surfaces. (b)-(e) The inner-sphere adsorption structures of $Li(DMSO)_n^+$ (n=3,2,1,0) on the Co_3O_4 (100)-O surfaces, together with their adsorption energies, respectively. ($\Delta G_{ads} = G_{inner-sphere}$ - $G_{outer-sphere}$).

After the first Li_2O_2 formed on the Co_3O_4 (100)-O surface, we found that the partial LiO_2 monomer (in *Li_2O_2 adsorbate) can be desorbed from the electrode surface to DMSO electrolyte. As shown in Fig. 5, we considered the LiO_2 desorption reaction ($\Delta G_{des} = G_{*Li} + G_{LiO_2(DMSO)_n}$ - $G_{*Li_2O_2}$ - n$\times$ G_{DMSO}, where n = 1, 2, 3, and 4) assisted with n explicit DMSO

molecules. We found that the desorption reaction is exothermic ($\Delta G_{\mathrm{des}} = -0.59$ eV) to form a three coordinated solvation structures, while the fourth explicit DMSO only slightly contributes to the LiO_2 desorption reaction, because it will not enter into the first solvation shell of $LiO_2(DMSO)_3$. The three-coordinated solvation structure of LiO_2 has also been reported by previous *ab initio* molecular dynamics simulations.[42] Therefore, we confirmed that the LiO_2 desorption reaction is favourable at the interface of Co_3O_4 (100)-O cathode and the DMSO electrolyte, which provides a special solution model (see below discussion) for discharging/charging processes in the Li-air batteries.

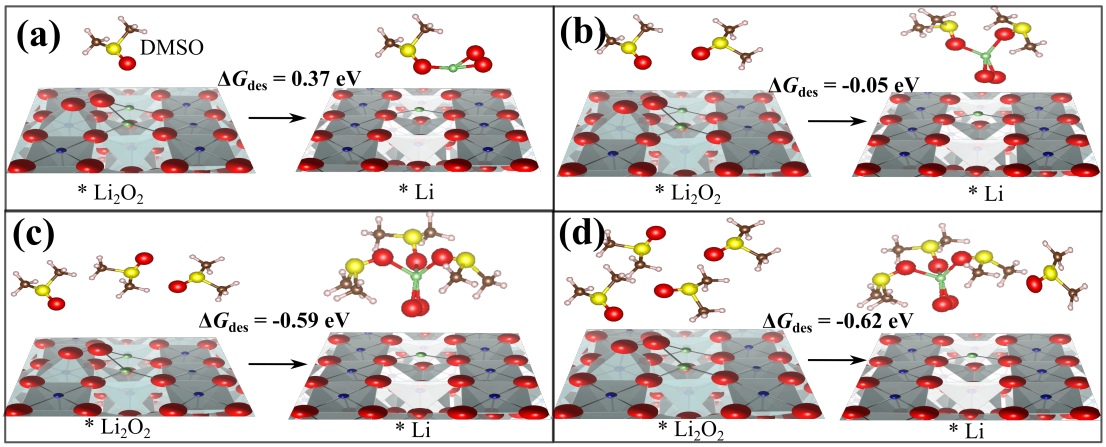

Figure 5: (a)-(d), the desorption of LiO_2 monomer from the Co_3O_4 (100) surface to DMSO electrolyte with the assistance of one-four explicit DMSO molecules, respectively.

Solution model for discharging/charging process at Co_3O_4 (100)-O electrode and DMSO electrolyte In the system of Co_3O_4 (100)-O electrode and DMSO electrolyte, the solution model is preferred due to the desorption of LiO_2 is thermodynamically favourable from the cathode to the electrolyte. Therefore, in Fig. 6(a), the general mechanism and overpotential for Li-O_2 discharge reactions at the interface of Co_3O_4 (100)-O cathode and DMSO eletrolyte is shown. The discharge pathways in such a system can be described into three main steps:

$$2\mathrm{Li}^+ + 2\mathrm{e}^- + \mathrm{O}_2(g) \xrightarrow{\text{discharge}} {}^*\mathrm{Li}_2\mathrm{O}_2 \qquad \text{(step I)}$$

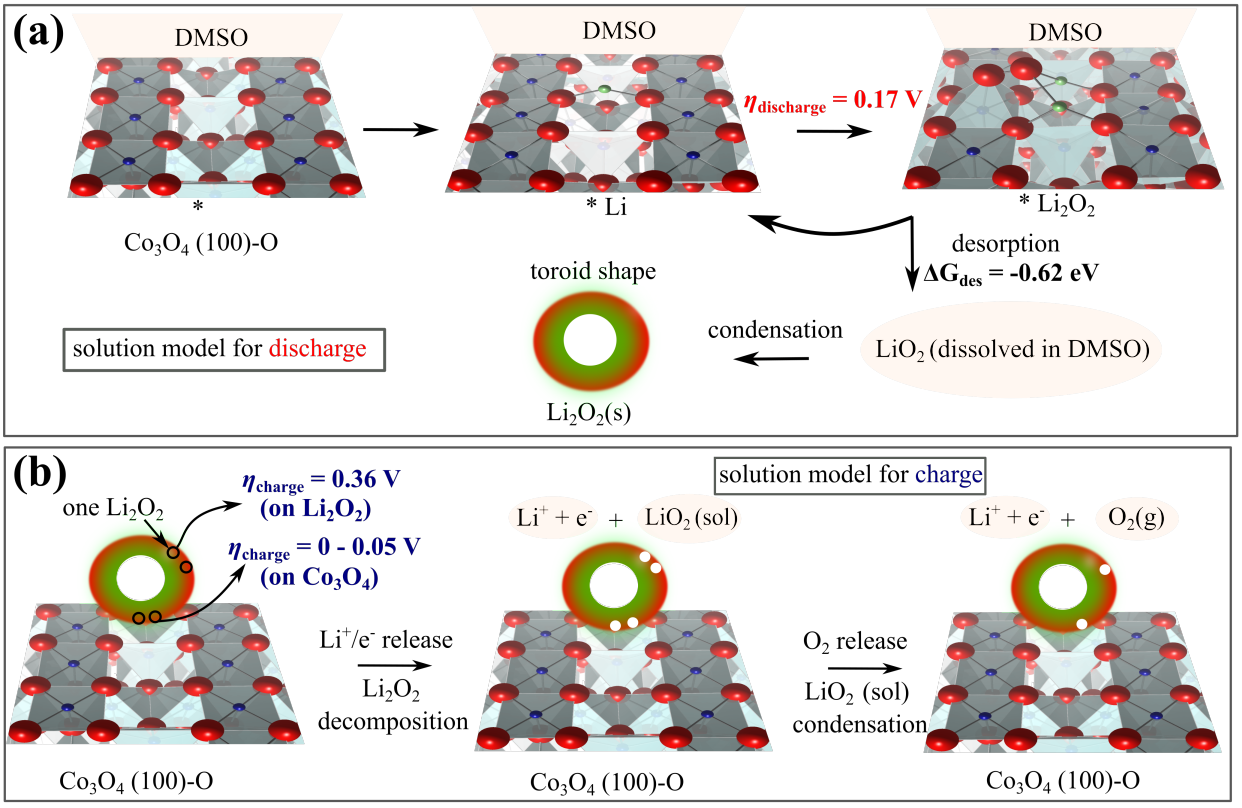

Figure 6: (a), the solution model pathway for discharge reactions on the Co_3O_4 (100)-O surfaces. The ΔG_{des} indicates the desorption free energy of LiO_2 monomer from the Co_3O_4 (100) surface to DMSO electrolyte shown in Fig. 5. (b), the solution model pathway for charge reactions on the Co_3O_4 (100)-O surfaces.

$$^{*}Li_2O_2 \xrightarrow{\text{desorption}} LiO_2(sol) + {}^{*}Li \qquad \text{(step II)}$$

$$2LiO_2(sol) \xrightarrow{\text{condensation}} Li_2O_2(s) + O_2(g) \qquad \text{(step III)}$$

Step I is to form a $^{*}Li_2O_2$ monomer on the cathode, showing a discharge overpotential of $\eta_{\text{discharge}} = 0.17$ V in Fig. 2(b)). Then, step II is to desorb one LiO_2 molecule from the cathode surface to DMSO electrolyte. When the concentration of LiO_2 (*sol*) increases in the electrolyte, the sparingly soluble Li_2O_2 will precipitate, contributing to growth of a toroidal particle (step III).[32,33,43,44] Furthermore, the active O-O bridge site on the Co_3O_4 (100)-O surface becomes available for the next $^{*}Li_2O_2$ formation (after LiO_2 desorbs at step II). As a result, the long-term surface discharge reaction will be $^{*}Li + Li^{+} + e^{-} + O_2 \rightarrow {}^{*}Li_2O_2$, providing a constant $\eta_{\text{discharge}} = 0.17$ V during the whole discharging process. Here, it is worth noting that the Steps I and II of our mechanisms are slightly different from the the steps of reaction (a) and (b) (see Introduction section) deduced from experiments. The reason is the formation of $^{*}Li$ intermediates is more favourable than that of $^{*}LiO_2$ intermediates on the Co_3O_4 (100)-O surface (see above mechanistic section). Therefore, the desorption of LiO_2 only proceeds after the whole $^{*}Li_2O_2$ monomer is formed on the Co_3O_4 (100)-O surface.

Fig. 6(b) shows the general solution model of the charge process (toroid Li_2O_2 (*s*) decomposition) at the interface of DMSO/Co_3O_4 (100)-O. We consider the decomposition from both the Li_2O_2 surface and the Co_3O_4 (100)-O surface. On the Co_3O_4 (100)-O surface, the $\eta_{\text{charge}} = 0$ V for the pathway of $^{*}Li_2O_2 \rightarrow {}^{*}Li + Li^{+} + e^{-} + O_2$ is obtained. Although this pathway provide a zero overpotential, the decomposition reaction is sluggish because almost all of the Li_2O_2 (*s*) particle surface area is neither resting on nor adjacent to the Co_3O_4 (100)-O surface. To accelerate the decomposition (i.e. make the charging process rapid), it is better to make the decomposition of Li_2O_2 favorable from its own surface. According to previous studies, the $\eta_{\text{charge}} = 0.36$ V is required for the decomposition reaction on the Li_2O_2 (0001)-O rich surface.[38] Therefore, a reasonable overpotential of 0.36 V is required for the fast charging process in such a system, where the decomposition of Li_2O_2 (*s*) will start

from both toroid Li_2O_2 and Co_3O_4 (100)-O surfaces together. The decomposition pathways shown in Fig. 6(b) can be summarized into the following two steps:

$$2Li_2O_2(s) \rightarrow 2Li^+ + 2e^- + 2LiO_2(sol) \quad \text{(step I)}$$

$$2LiO_2(sol) \rightarrow Li_2O_2(s) + O_2(g) \quad \text{(step II)}$$

Finally, it is worth noting that our calculated $\eta_{\text{discharge}} = 0.17$ V (on Co_3O_4 (100)-O surface) is in a good agreement with experimental $\eta_{\text{discharge}} \approx 0.1$-$0.3$ V on Co_3O_4 particles.[16,20,45] However, the predicted overpotential of 0.36 V for Li_2O_2(s) decomposition is much smaller than the reported $\eta_{\text{charge}} \approx 1$ V in the experiment.[16,20,45] Moreover, according to previous experimental reports, $\eta_{\text{charge}} > 1$ V was found on most of the other cathode materials in Li-air batteries,[16] although the η_{charge} demand is found in a range of 0.2-0.6 V for Li_2O_2 decomposition (from all facets of Li_2O_2 crystal) even without any catalyst.[38,40] This theoretical and experimental η_{charge} discrepancy is due to the potential required to decompose the side product of lithium carbonate (including Li_2CO_3) formed during discharge, which has been detected as the main side product on many transition-metal oxides (including Co_3O_4).[45,46] The decomposition voltage of lithium carbonate is about 4.0-4.5 V (vs. RHE) in experiment,[46,47] which corresponds to a $\eta_{\text{charge}} \approx$ 1-1.5 V in Li-air battery. Therefore, in order to decrease the large η_{charge} (towards Li-air batteries) observed in realistic battery prototypes, it is more important to deal with the formation of side-product lithium carbonate rather than the decomposition of Li_2O_2 on the Co_3O_4 cathode.

Conclusion

In this paper, a systematic first-principles thermodynamic study of Li-air batteries consisted of Co_3O_4-cathode and DMSO-electrolyte is performed. We have investigated the surface structure, stable reconstructions, and the electronic properties of Co_3O_4. The Co_3O_4 (100)-

O surface is found to be the most stable one at standard conditions and all conditions in the bulk Co_3O_4 stability region. The Li^+ solvation structure in the DMSO-based electrolyte is determined as a tetrahedral $Li(DMSO)_4^+$ solvation shell by 25 ps *ab initio* molecular dynamics (AIMD) equlibrations. Once a $*Li_2O_2$ discharge product is formed on the cathode surface, the partial LiO_2 monomer is found energetically favourable to be desorbed into the DMSO solvent leaving empty active sites (on the cathode surface) for the next $*Li_2O_2$ product formation. As a result, in such a system of Co_3O_4 (100)-O surface and DMSO solvent, the discharge reactions follow a solution model with a constant $\eta_{\text{discharge}} = 0.17$ V. Meanwhile, a 0.36 V overpotential is required to decompose Li_2O_2 from itself surface in order to get a rapid charging process. The higher $\eta_{\text{charge}} \approx 1$ V observed in experiment is due to the voltage demand to decompose the side product lithium carbonate (including Li_2CO_3) formed during discharge. Besides that, the kinetic barriers of the interface adsorption/desorption process also limit the overall efficiency of the Li-air batteries, which requires more studies in the future. In general, the present study shows that low $\eta_{\text{discharge}}$ is achievable and understandable, avoiding the formation of side products on Co_3O_4 in order to reduce η_{charge} is one of the main technical challenges on the road to efficient Li-air batteries.

Acknowledgement

Z.J. and A.M.R. acknowledge support from the U.S. Department of Energy, Office of Science, Basic Energy Sciences, under Award # DE-SC0019281. The authors thank Tian Qiu for help with the *ai*-GCMC calculations, and Arvin Kakekhani for meaningful discussions. Computational support was provided by the National Energy Research Scientific Computing Center (NERSC), a U.S. Department of Energy, Office of Science User Facility located at Lawrence Berkeley National Laboratory, operated under Contract No. DE-AC02-05CH11231.

Supporting Information Available

The computational details can be found in the Supporting Information. The less energetic favourable mechanism for the Li + O_2 reactions on the Co_3O_4 (100)-O surface can also be found in the Supporting Information. In addition, the results and discussion about the Li + O_2 reactions on the Co_3O_4 (100)-S and (100)-R surfaces are also included there.

References

(1) Goodenough, J. B.; Park, K.-S. The Li-ion rechargeable battery: a perspective. *J. Am. Chem. Soc.* **2013**, *135*, 1167–1176.

(2) Bonaccorso, F.; Colombo, L.; Yu, G.; Stoller, M.; Tozzini, V.; Ferrari, A. C.; Ruoff, R. S.; Pellegrini, V. Graphene, related two-dimensional crystals, and hybrid systems for energy conversion and storage. *Science* **2015**, *347*.

(3) Li, M.; Qiu, T.; Foucher, A. C.; Fu, J.; Wang, Z.; Zhang, D.; Rappe, A. M.; Stach, E. A.; Detsi, E. Impact of Hierarchical Nanoporous Architectures on Sodium Storage in Antimony-Based Sodium-Ion Battery Anodes. *ACS Appl. Energy Mater.* **2020**, *3*, 11231–11241.

(4) Jiang, Z.; Alexandrov, V. Electrocatalytic activity of oxygen-functionalized carbon electrodes for vanadium redox flow batteries from free-energy calculations. *ACS Appl. Energy Mater.* **2020**, *3*, 7543–7549.

(5) Xu, Y.; Shelton, W. A. O_2 reduction by lithium on Au (111) and Pt (111). *J. Chem. Phys.* **2010**, *133*, 024703.

(6) Li, X.; Gu, M.; Hu, S.; Kennard, R.; Yan, P.; Chen, X.; Wang, C.; Sailor, M. J.; Zhang, J.-G.; Liu, J. Mesoporous silicon sponge as an anti-pulverization structure for high-performance lithium-ion battery anodes. *Nat. Commun.* **2014**, *5*, 1–7.

(7) Intan, N. N.; Klyukin, K.; Alexandrov, V. Ab initio modeling of transition metal dissolution from the $LiNi_{0.5}Mn_{1.5}O_4$ cathode. *ACS Appl. Mater. Interfaces* **2019**, *11*, 20110–20116.

(8) Luntz, A. C.; McCloskey, B. D. Nonaqueous Li-air batteries: a status report. *Chem. Rev.* **2014**, *114*, 11721–11750.

(9) Lim, H.-D.; Lee, B.; Bae, Y.; Park, H.; Ko, Y.; Kim, H.; Kim, J.; Kang, K. Reaction chemistry in rechargeable Li-O_2 batteries. *Chem. Soc. Rev.* **2017**, *46*, 2873–2888.

(10) Kondori, A.; Jiang, Z.; Esmaeilirad, M.; Tamadoni Saray, M.; Kakekhani, A.; Kucuk, K.; Navarro Munoz Delgado, P.; Maghsoudipour, S.; Hayes, J.; Johnson, C. S., et al. Kinetically Stable Oxide Overlayers on Mo_3P Nanoparticles Enabling Lithium-Air Batteries with Low Overpotentials and Long Cycle Life. *Adv. Mater.* **2020**, *32*, 2004028.

(11) Zhang, X.; Chen, A.; Jiao, M.; Xie, Z.; Zhou, Z. Understanding Rechargeable Li-O_2 Batteries via First-Principles Computations. *Batteries Supercaps* **2019**, *2*, 498–508.

(12) Zhang, P.; Zhao, Y.; Zhang, X. Functional and stability orientation synthesis of materials and structures in aprotic Li-O_2 batteries. *Chem. Soc. Rev.* **2018**, *47*, 2921–3004.

(13) Aurbach, D.; McCloskey, B. D.; Nazar, L. F.; Bruce, P. G. Advances in understanding mechanisms underpinning lithium-air batteries. *Nat. Energy* **2016**, *1*, 1–11.

(14) Tamakloe, W.; Agyeman, D. A.; Park, M.; Yang, J.; Kang, Y.-M. Polydopamine-induced surface functionalization of carbon nanofibers for Pd deposition enabling enhanced catalytic activity for the oxygen reduction and evolution reactions. *J. Mater. Chem. A* **2019**, *7*, 7396–7405.

(15) Wang, C.; Xie, Z.; Zhou, Z. Lithium-air batteries: Challenges coexist with opportunities. *APL Mater.* **2019**, *7*, 040701.

(16) Surya, K.; Michael, M.; Prabaharan, S. A review on advancement in non-noble metal based oxides as bifunctional catalysts for rechargeable non-aqueous Li/air battery. *Solid State Ion.* **2018**, *317*, 89–96.

(17) Wang, J.; Gao, R.; Zhou, D.; Chen, Z.; Wu, Z.; Schumacher, G.; Hu, Z.; Liu, X. Boosting the electrocatalytic activity of Co_3O_4 nanosheets for a Li-O_2 battery through modulating inner oxygen vacancy and exterior Co^{3+}/Co^{2+} ratio. *ACS Catal.* **2017**, *7*, 6533–6541.

(18) Gao, R.; Yang, Z.; Zheng, L.; Gu, L.; Liu, L.; Lee, Y.; Hu, Z.; Liu, X. Enhancing the catalytic activity of Co_3O_4 for Li-O2 batteries through the synergy of surface/interface/doping engineering. *ACS Catal.* **2018**, *8*, 1955–1963.

(19) Gao, R.; Shang, Z.; Zheng, L.; Wang, J.; Sun, L.; Hu, Z.; Liu, X. Enhancing the Catalytic Activity of Co3O4 Nanosheets for Li-O_2 Batteries by the Incoporation of Oxygen Vacancy with Hydrazine Hydrate Reduction. *Inorg. Chem.* **2019**, *58*, 4989–4996.

(20) Cui, Y.; Wen, Z.; Sun, S.; Lu, Y.; Jin, J. Mesoporous Co_3O_4 with different porosities as catalysts for the lithium–oxygen cell. *Solid State Ion.* **2012**, *225*, 598–603.

(21) Xiao, Z.; Huang, Y.-C.; Dong, C.-L.; Xie, C.; Liu, Z.; Du, S.; Chen, W.; Yan, D.; Tao, L.; Shu, Z., et al. Operando identification of the dynamic behavior of oxygen vacancy-rich Co_3O_4 for oxygen evolution reaction. *J. Am. Chem. Soc.* **2020**, *142*, 12087–12095.

(22) Zasada, F.; Piskorz, W.; Sojka, Z. Cobalt spinel at various redox conditions: DFT + U investigations into the structure and surface thermodynamics of the (100) facet. *J. Phys. Chem. C* **2015**, *119*, 19180–19191.

(23) Xu, X.-L.; Chen, Z.-H.; Li, Y.; Chen, W.-K.; Li, J.-Q. Bulk and surface properties of spinel Co_3O_4 by density functional calculations. *Surf. Sci.* **2009**, *603*, 653–658.

(24) Shojaee, K.; Montoya, A.; Haynes, B. S. Insight into oxygen stability and vacancy formation on Co_3O_4 model slabs. *Comput. Mater. Sci* **2013**, *72*, 15–25.

(25) Montoya, A.; Haynes, B. S. Periodic density functional study of Co_3O_4 surfaces. *Chem. Phys. Lett.* **2011**, *502*, 63–68.

(26) Lyu, Z.; Yang, L.; Luan, Y.; Wang, X. R.; Wang, L.; Hu, Z.; Lu, J.; Xiao, S.; Zhang, F.; Wang, X., et al. Effect of oxygen adsorbability on the control of Li_2O_2 growth in Li-O_2 batteries: Implications for cathode catalyst design. *Nano Energy* **2017**, *36*, 68–75.

(27) Dathar, G. K. P.; Shelton, W. A.; Xu, Y. Trends in the catalytic activity of transition metals for the oxygen reduction reaction by lithium. *J. Phys. Chem. Lett.* **2012**, *3*, 891–895.

(28) Novčić, K. A.; Dobrota, A. S.; Petković, M.; Johansson, B.; Skorodumova, N. V.; Mentus, S. V.; Pašti, I. A. Theoretical analysis of doped graphene as cathode catalyst in Li-O_2 and Na-O_2 batteries-the impact of the computational scheme. *Electrochim. Acta* **2020**, *354*, 136735.

(29) Jing, Y.; Zhou, Z. Computational insights into oxygen reduction reaction and initial Li_2O_2 nucleation on pristine and N-doped graphene in Li–O_2 batteries. *ACS Catal.* **2015**, *5*, 4309–4317.

(30) Ganapathy, S.; Adams, B. D.; Stenou, G.; Anastasaki, M. S.; Goubitz, K.; Miao, X.-F.; Nazar, L. F.; Wagemaker, M. Nature of Li_2O_2 oxidation in a Li-O_2 battery revealed by operando X-ray diffraction. *J. Am. Chem. Soc.* **2014**, *136*, 16335–16344.

(31) Liu, C.; Brant, W. R.; Younesi, R.; Dong, Y.; Edström, K.; Gustafsson, T.; Zhu, J. Towards an Understanding of Li_2O_2 Evolution in Li-O_2 Batteries: An In Operando Synchrotron X-ray Diffraction Study. *ChemSusChem* **2017**, *10*, 1592–1599.

(32) Lyu, Z.; Zhou, Y.; Dai, W.; Cui, X.; Lai, M.; Wang, L.; Huo, F.; Huang, W.; Hu, Z.; Chen, W. Recent advances in understanding of the mechanism and control of Li_2O_2 formation in aprotic Li-O_2 batteries. *Chem. Soc. Rev.* **2017**, *46*, 6046–6072.

(33) Johnson, L.; Li, C.; Liu, Z.; Chen, Y.; Freunberger, S. A.; Ashok, P. C.; Praveen, B. B.; Dholakia, K.; Tarascon, J.-M.; Bruce, P. G. The role of LiO_2 solubility in O_2 reduction in aprotic solvents and its consequences for Li–O_2 batteries. *Nat. Chem.* **2014**, *6*, 1091–1099.

(34) Lai, J.; Xing, Y.; Chen, N.; Li, L.; Wu, F.; Chen, R. Electrolytes for Rechargeable Lithium-Air Batteries. *Angew. Chem. Int. Ed.* **2020**, *59*, 2974–2997.

(35) Wexler, R. B.; Qiu, T.; Rappe, A. M. Automatic Prediction of Surface Phase Diagrams Using Ab Initio Grand Canonical Monte Carlo. *J. Phys. Chem. C* **2019**, *123*, 2321–2328.

(36) Wang, L.; Maxisch, T.; Ceder, G. Oxidation energies of transition metal oxides within the GGA + U framework. *Phys. Rev. B* **2006**, *73*, 195107.

(37) Walsh, A.; Wei, S.-H.; Yan, Y.; Al-Jassim, M.; Turner, J. A.; Woodhouse, M.; Parkinson, B. Structural, magnetic, and electronic properties of the Co-Fe-Al oxide spinel system: Density-functional theory calculations. *Phys. Rev. B* **2007**, *76*, 165119.

(38) Hummelshøj, J.; Luntz, A.; Nørskov, J. Theoretical evidence for low kinetic overpotentials in Li-O_2 electrochemistry. *J. Chem. Phys.* **2013**, *138*, 034703.

(39) Viswanathan, V.; Thygesen, K. S.; Hummelshøj, J.; Nørskov, J. K.; Girishkumar, G.; McCloskey, B.; Luntz, A. Electrical conductivity in Li_2O_2 and its role in determining capacity limitations in non-aqueous Li-O_2 batteries. *J. Chem. Phys.* **2011**, *135*, 214704.

(40) Mo, Y.; Ong, S. P.; Ceder, G. First-principles study of the oxygen evolution reaction of lithium peroxide in the lithium-air battery. *Phys. Rev. B* **2011**, *84*, 205446.

(41) Li, X.; Li, Z.; Yang, X.; Jia, L.; Fu, Y. Q.; Chi, B.; Pu, J.; Li, J. First-principles study of the initial oxygen reduction reaction on stoichiometric and reduced CeO_2 (111) surfaces as a cathode catalyst for lithium–oxygen batteries. *J. Mater. Chem. A* **2017**, *5*, 3320–3329.

(42) Scheers, J.; Lidberg, D.; Sodeyama, K.; Futera, Z.; Tateyama, Y. Life of superoxide in aprotic Li-O_2 battery electrolytes: simulated solvent and counter-ion effects. *Phys. Chem. Chem. Phys.* **2016**, *18*, 9961–9968.

(43) Zeng, J.; Francia, C.; Amici, J.; Bodoardo, S.; Penazzi, N. A highly reversible Li–O_2 battery utilizing a mixed electrolyte and a cathode incorporating Co_3O_4. *RSC Adv.* **2015**, *5*, 83056–83064.

(44) Aetukuri, N. B.; McCloskey, B. D.; García, J. M.; Krupp, L. E.; Viswanathan, V.; Luntz, A. C. Solvating additives drive solution-mediated electrochemistry and enhance toroid growth in non-aqueous Li–O_2 batteries. *Nat. chem.* **2015**, *7*, 50–56.

(45) Lim, H.-D.; Gwon, H.; Kim, H.; Kim, S.-W.; Yoon, T.; Choi, J. W.; Oh, S. M.; Kang, K. Mechanism of Co_3O_4/graphene catalytic activity in Li-O_2 batteries using carbonate based electrolytes. *Electrochim. Acta* **2013**, *90*, 63–70.

(46) Balaish, M.; Jung, J.-W.; Kim, I.-D.; Ein-Eli, Y. A Critical Review on Functionalization of Air-Cathodes for Nonaqueous Li-O_2 Batteries. *Adv. Funct. Mater.* **2020**, *30*, 1808303.

(47) Seong, W. M.; Cho, K.-H.; Park, J.-W.; Park, H.; Eum, D.; Lee, M. H.; Kim, I.-s. S.; Lim, J.; Kang, K. Controlling residual lithium in high-nickel (>90%) lithium layered oxides for cathodes in lithium-ion batteries. *Angew. Chem. Int. Ed.* **2020**, *59*, 18662–18669.

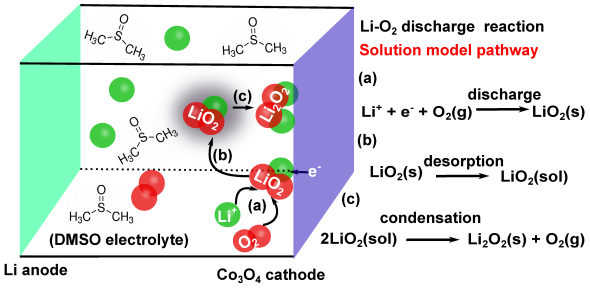

Li-O_2 discharge reaction

Solution model pathway

(a)

$Li^+ + e^- + O_2(g) \xrightarrow{\text{discharge}} LiO_2(s)$

(b)

$LiO_2(s) \xrightarrow{\text{desorption}} LiO_2(sol)$

(c)

$2LiO_2(sol) \xrightarrow{\text{condensation}} Li_2O_2(s) + O_2(g)$